Field Intercomparison of Nearshore Directional Wave Sensors

WILLIAM G. GROSSKOPF, DAVID G. AUBREY, MICHAEL G. MATTIE, AND MARTIN MATHIESEN

(Invited Paper)

***Abstract*—Five measurement strategies (four *in situ*, one remote) for estimating directional wave spectra were intercompared in a 1980 experiment at the Coastal Engineering Research Center's Field Research Facility in Duck, NC. The systems included two pressure sensor/biaxial current meter combinations (different manufacturers), a triaxial acoustic current meter, an SXY gauge (square array of four pressure sensors), and a shore-based imaging radar. A detailed error analysis suggests sources for differences in estimated wave spectra from the different instruments; in general, they intercompare favorably. The major deviation among *in situ* gauges was associated with the triaxial acoustic current meter. Reliance on a vertical velocity measurement (instead of a direct pressure or sea-surface elevation measurement) can contribute additional uncertainty in directional spectral estimates. The imaging radar was successful in distinguishing multiple wave trains at the same frequency, which was not possible with the simple spectral estimation analysis applied to *in situ* data. However, the radar is not useful in providing accurate estimates of spectral density, nor in distinguishing multiple wave trains of different frequencies coming from the same direction. Selection of a measurement strategy for a particular need depends on the precise data requirements for that application. Although the five tested intercompared well, in practice not all are equally suitable for every application.**

I. INTRODUCTION

DURING THE months of October and November, 1980, the Atlantic Remote Sensing Land Ocean Experiment (ARSLOE) was held at the U.S. Army Coastal Engineering Research Center (CERC) Field Research Facility (FRF), at Duck, NC (Fig. 1). The ARSLOE experiment was organized and conducted by the Coastal Engineering Research Center (CERC) and the National Ocean Survey Coastal Wave Program. An overview of the total experiment, as well as a discussion of the motivation for the experiment is provided by Baer and Vincent [17]. This experiment was organized primarily to evaluate the use of various types of remote sensing devices in the measurement of ocean wave characteristics with verification using data collected by *in situ* devices. Additional emphasis was focused on the capability of wave gauging devices and analysis techniques to accurately represent directional wave properties in shallow water. This paper presents a comparison of measurements from four *in situ* wave gauges and one remote sensing device deployed in the the vicinity of the FRF pier during ARSLOE.

The comparisons presented in this paper include directional wave estimates from: a) a triaxial acoustic current meter (NHL UVW) deployed and analyzed by the Norwegian Hydrodynamic Laboratories, b) a biaxial current/pressure gauge combination (CERC UVP) deployed and analyzed by the Coastal Engineering Research Center, c) a shore-based wave imaging radar deployed and analyzed by CERC, d) a biaxial current meter/pressure gauge combination (WHOI UVP) deployed and analyzed by Woods Hole Oceanographic Institution, and e) an SXY gauge (an array of four pressure gauges configured in a square pattern) deployed for CERC and analyzed by Scripps Oceanographic Institution (Table I). A third biaxial current meter/pressure gauge combination (Marsh-McBirney 585) and a three-element linear pressure sensor array also operated during ARSLOE. The Marsh-McBirney 585 did not work during the experiment; results from the linear array were not available at the time of this writing. All *in situ* devices (i.e., instruments a, b, d, e) provide spectral estimates of wave height, frequency, and direction, whereas imaging radar provides only frequency and direction information. Surface wave height and peak frequency comparisons were also made with a pier-based Baylor wave gauge. Results from this study illustrate the comparability not only of different instruments and measurement strategies at slightly different locations, but also of analysis procedures (Table II).

II. FIELD SITE

The instruments under comparison in this paper were all installed on or near the end of the FRF pier during ARSLOE (Fig. 2). The pier is located on the coast of the Outer Banks of North Carolina at Duck (Fig. 1), approximately 100 km south of Virginia Beach, VA. Fig. 2 shows the locations of the shallow water wave gauges compared in this paper. The ground-based radar was located on the pier end, while *in situ* devices were deployed about 150 m north

Manuscript received March 16, 1983; revised July 22, 1983. The second author was supported from a number of different sources for his part in the work: the field aspect was funded by Exxon Production Research Company under Technical Services agreement PR-6520 to Sea Data Corporation; the remainder of his work was supported by the Department of Commerce under Grant NA79AA-D-00102, the NOAA Office of Sea Grant under Grant NA80AA-D-00077, and U.S. Army Research Office under Contract DAAG29-81-K-0004. This is Woods Hole Oceanographic Institution Contribution number 5222.

W. G. Grosskopf was with the Coastal Engineering Research Center, Fort Belvoir, VA. He is now with ARCTEC, Inc., Columbia, MD 21045.

D. G. Aubrey is with Woods Hole Oceanographic Institution, Woods Hole, MA 02543.

M. G. Mattie was with the Coastal Engineering Research Center, Fort Belvoir, VA. He is now with the Engineering Topographic Laboratory, Fort Belvoir, VA 22060.

M. Mathiesen is with the Norwegian Hydrodynamic Laboratories, Trondheim, Norway.

0364-9059/83/1000-0254$01.00

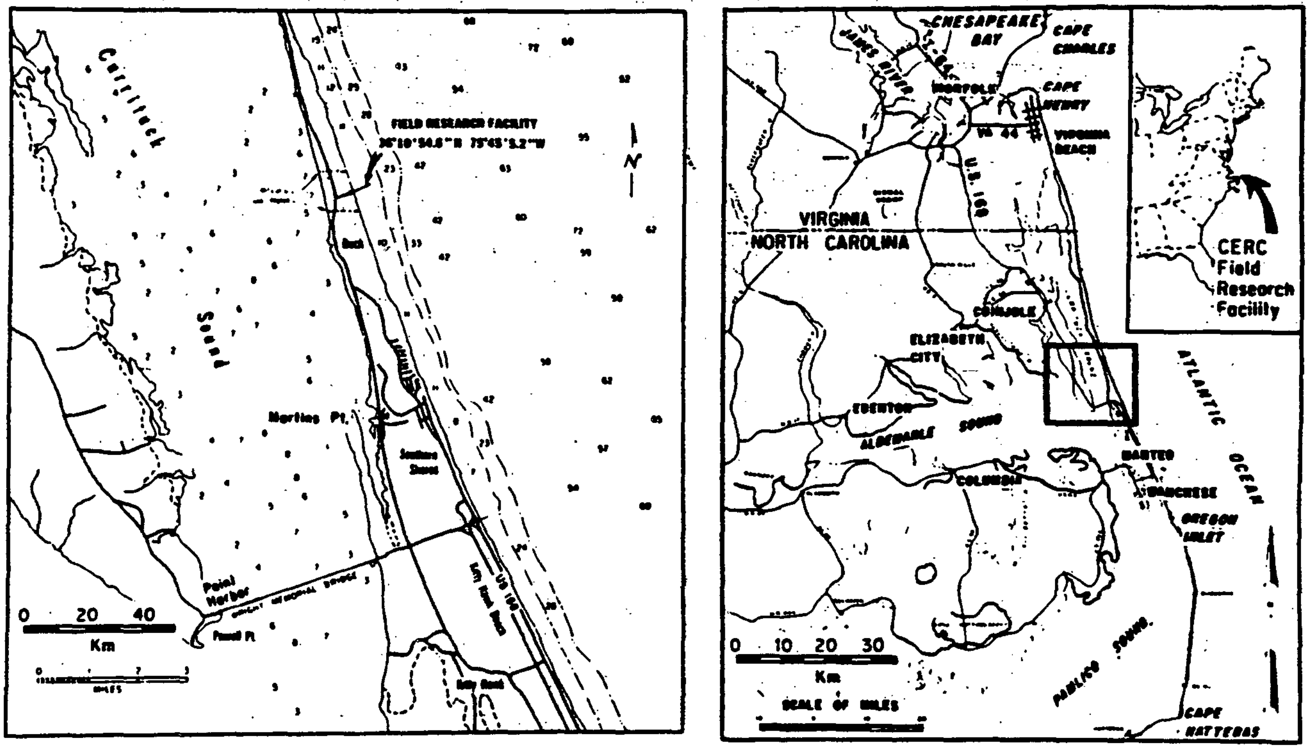

Fig. 1. Location of the coastal engineering research center's field research facility (FRF), Duck, NC.

TABLE I
SUMMARY OF SHALLOW WATER WAVE DIRECTION GAUGES DEPLOYED DURING ARSLOE

Gauge	a	b	c	d	e
Instrument/ Sponsor	Triaxial Current Meter/Norwegian Hydrodynamic Laboratories	Biaxial Current Meter Pressure Gauge/Coastal Engineering Research Center	*X*-Band Surface Imaging Radar/Coastal Engineering Research Center	Biaxial Current Meter Pressure Gauge/Woods Hole Oceanographic Institution	SXY Gauge/Coastal Engineering Research Center
Model/Manufacturer	Model UCM-2/ Christian Michelsen Institute, Bergen, Norway	Model 551/Marsh McBirney Current with Bell and Howell pressure	Raytheon 1020/9xR Mariners Pathfinder *X*-band radar	Model 635-9/Sea Data Corporation, Newton, MA	Assembled by Scripps Institution of Oceanography
Operating Principle	Acoustic travel time difference	March–McBirney Electromagnetic Current Meter/Strain Gauge (Kulite)	Detects backscattered energy from water surface	Marsh–McBirney Electromagnetic Current Meter/ Digiquartz pressure transducer	Strain Gauge (Kulite)
Averaging Length or Diameter of Velocity Sensor	~10 cm	10.2 cm	NA	3.8 cm	NA
Resolution of Velocity Estimates	0.12 cm/s	1.2 cm/s	NA	0.3 cm/s	NA
Accuracy of Velocity Estimates	UNKNOWN	Greater of 2 cm/s or 2 percent (manufacturers numbers)	NA	1 percent of Signal (Based on calibration results)	NA
Resolution of Pressure Measurements	NA	1–3 mm	NA	0.5 mm	1–3 mm
Accuracy of Pressure Measurements	NA	1–2 cm (short-term, relative accuracy)	NA	1.5 mm	1–2 cm (short-term, relative accuracy)
Compass	YES	NONE	NONE	DIGICOURSE	NONE
Vertical Sense	Diver-Oriented	Diver-Oriented	NA	Diver-Oriented	NONE

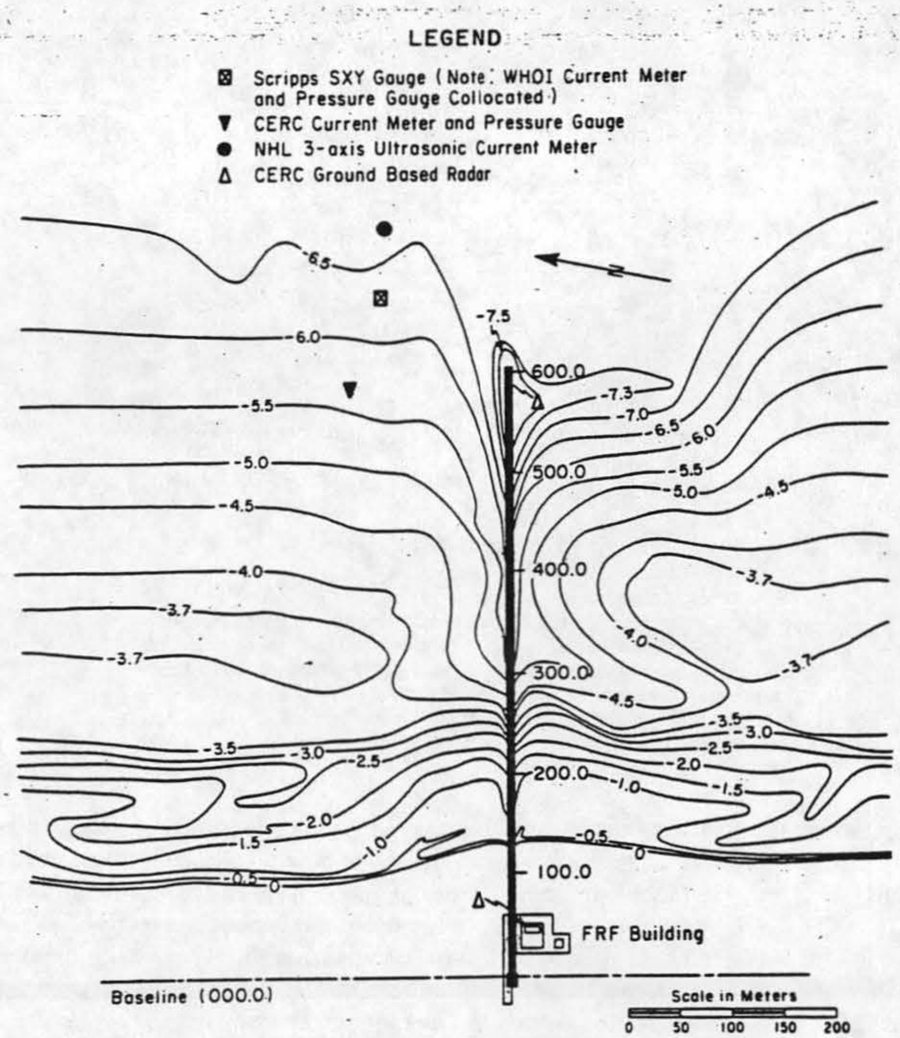

Fig. 2. Location of ARSLOE shallow water wave directional gauges compared in this paper.

TABLE II
SUMMARY OF SHALLOW WATER WAVE DIRECTION GAUGES DEPLOYED DURING ARSLOE

Gauge	a	b	c	d	e
Recording Method	Internal cassette	Cable to shore, recorded by computer	Photograph CRT using Bolex 16-mm H-16 reflex camera	Internal cassette	Cable to shore, recorded by computer
Sampling	1 Hz	4 Hz	Sweep time 1.8 s	1 Hz	1 Hz
Collection Interval	4 h	Continuously for high seas, otherwise 6 h	Hourly or twice	6 h	6 h
Record Length for Analysis	1024 s	1024 s	36 sweeps per collection interval	2048 s	1024 s
Operating times 1980	Oct. 10 17:15–Oct. 29 05:15 GMT Oct. 31 21:15–Nov. 7 09:15 GMT	Continuously through ARSLOE	Continuously through ARSLOE	Oct. 31 18:00–Nov. 24 12:00 GMT	Continuously through ARSLOE
Reference	Mathieson and Faanes (1982)	Grosskopf (1981)	Mattie & Harris (1979)	Aubrey (1981)	Seymour & Higgins (1978)
Bandwidth	.00781 Hz	0.00781 Hz	5–10 percent in wavelength (bandwidth is depth dependent) dependent)	0.00781 Hz	0.01562 Hz
Window Function	10 percent cosine bell taper at beginning and end of record	Full cosine bell	NA	Box car	Box car
Degrees of Freedom	16	16	NA	32	32

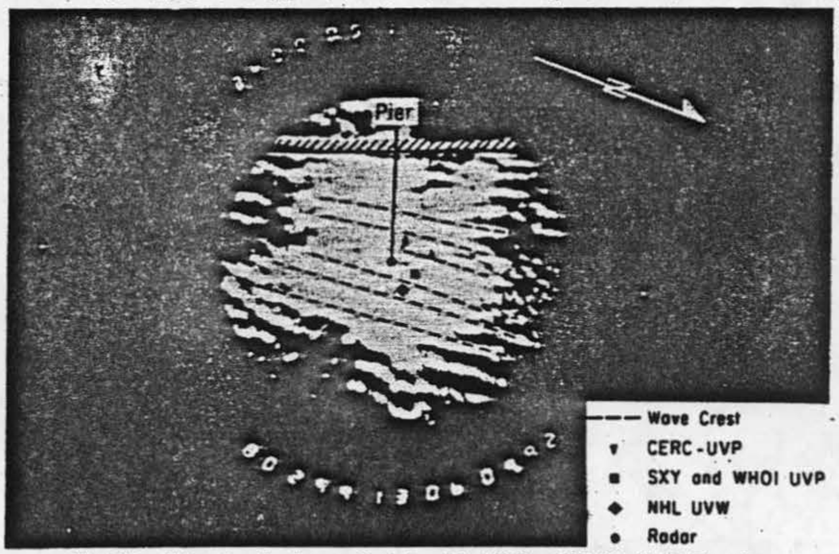

Fig. 3. *X*-band radar image October 25, 1980, at 17:00 GMT. Turning of crests is evident during this case of extremely high wave conditions. Approximate locations of the gauges indicate that the effects of the pier and bathymetry could have some effect on wave directional measurements; however the gauges appear to be situated outside the area of major pier effects. Less effect of the pier and bathymetry is noted when wave energy is lower and direction is less southerly.

of the pier end away from the area where the bottom contours are irregular. *In situ* instruments were in mean water depths ranging from 5.7 to 7.0 m, referenced to mean low water.

Some spatial variability in the wave field occurs in the area adjacent to the pier where the gauges are located, due to wave shoaling phenomena. Refraction and diffraction in this area will contribute to differences in wave direction as measured by the spatially distributed instruments. The effect of this spatial variability in wave direction (graphically shown in radar imagery—Fig. 3) is greatest for waves propagating from the south over the depression near the end of the pier. Energy sinks in this shallow water region causing spatial variability include bottom friction, percolation, and wave dissipation; these may affect coherence of results. Energy transfers between wave frequencies due to nonlinear shallow water wave interaction may affect intercomparability. Since all instruments are located close together, fetch differences are not important.

The FRF pier contributes an additional physical effect. The unusual bathymetry around the pier due to the 600-m-long structure may provide a consistent bias to directional intercomparisons; short-term pier effects such as interruptions in longshore current structure, offshore-directed jets beneath or alongside the pier, and disruptions in the wave patterns by the pilings may also cause slight differences in the wave field between gauge locations.

III. DIRECTIONAL DATA COLLECTION AND ANALYSIS

A. Theoretical Approaches for Analyzing In Situ Data

Three types of *in situ* wave directional gauges are included in this comparison: UVP gauges which collect two horizontal current components and dynamic wave pressure data, a UVW gauge which collects all three current components, and an SXY gauge which collects dynamic wave pressure data at the four corners of a 6.1- × 6.1-m square frame placed on the seabed. Data reduction for each of the gauges relies on separate data analysis programs built around theories which are basically similar but do contain some differences which can affect intercomparison of gauge measurements.

Computations of wave direction for the *in situ* gauges in this comparison are based upon methods analogous to those presented by Longuet-Higgins *et al.* [8] for a heave-pitch-roll buoy. The water surface displacement $\eta(x, y, t)$ is given by

$$\eta(x, y, t) = \int_{-\infty}^{\infty} \int_{0}^{2\pi} F(\sigma, \theta) e^{i(\sigma t - k_x x - k_y y)} \, d\theta \, d\sigma \quad (1)$$

where $F(\sigma, \theta)$ is the amplitude spectrum of the wave field as a function of frequency σ and direction θ. The dynamic wave pressure p, the horizontal water particle velocities u and v in the x and y directions, and the vertical water particle velocity w are related to $F(\sigma, \theta)$ according to linear wave theory

$$p(x, y, z, t) = \int_{-\infty}^{\infty} \int_{0}^{2\pi} F(\sigma, \theta) \gamma \frac{\cosh k(h + z)}{\cosh kh} \cdot e^{i(\sigma t - k_x x - k_y y)} \, d\theta \, d\sigma \quad (2)$$

$$u(x, y, z, t) = \int_{-\infty}^{\infty} \int_{0}^{2\pi} F(\sigma, \theta) \sigma \cos\theta \frac{\cosh k(h + z)}{\sinh kh} \cdot e^{i(\sigma t - k_x x - k_y y)} \, d\theta \, d\sigma \quad (3)$$

$$v(x, y, z, t) = \int_{-\infty}^{\infty} \int_{0}^{2\pi} F(\sigma, \theta) \sigma \sin\theta \frac{\cosh k(h + z)}{\sinh kh} \cdot e^{i(\sigma t - k_x x - k_y y)} \, d\theta \, d\sigma \quad (4)$$

$$w(x,y,z,t) = \int_{-\infty}^{\infty} \int_{0}^{2\pi} F(\sigma,\theta)\sigma \frac{\sinh k(h+z)}{\sinh kh} \cdot e^{i(\sigma t - k_x x - k_y y)}\, d\theta\, d\sigma \qquad (5)$$

where z is vertical (measured positive upward from mean water level), $\gamma = \rho g$ is specific gravity, ρ is water density, g is gravitational acceleration, k is wave number, h is water depth, and t is time.

Auto- and cross-spectra are obtained from (2)–(5)

$$S_{pp}(\sigma) = \int_0^{2\pi} K_p^2(\sigma) |F(\sigma,\theta)|^2 \, d\theta \qquad (6)$$

$$S_{uu}(\sigma) = \int_0^{2\pi} K_u^2(\sigma) \cos^2\theta \, |F(\sigma,\theta)|^2 \, d\theta = \int_0^{2\pi} K_u^2(\sigma) \left(\frac{1+\cos 2\theta}{2}\right) |F(\sigma,\theta)|^2 \, d\theta \qquad (7)$$

$$S_{vv}(\sigma) = \int_0^{2\pi} K_u^2(\sigma) \sin^2\theta \, |F(\sigma,\theta)|^2 \, d\theta = \int_0^{2\pi} K_u^2(\sigma) \left(\frac{1-\cos 2\theta}{2}\right) |F(\sigma,\theta)|^2 \, d\theta \qquad (8)$$

$$S_{ww}(\sigma) = \int_0^{2\pi} K_w^2(\sigma) |F(\sigma,\theta)|^2 \, d\theta \qquad (9)$$

$$S_{pu}(\sigma) = \int_0^{2\pi} K_p(\sigma) K_u(\sigma) \cos\theta \, |F(\sigma,\theta)|^2 \, d\theta \qquad (10)$$

$$S_{pv}(\sigma) = \int_0^{2\pi} K_p(\sigma) K_u(\sigma) \sin\theta \, |F(\sigma,\theta)|^2 \, d\theta \qquad (11)$$

$$S_{uv}(\sigma) = \int_0^{2\pi} K_u^2(\sigma) \sin\theta \cos\theta \, |F(\sigma,\theta)|^2 \, d\theta = \int_0^{2\pi} K_u^2(\sigma) \left(\frac{\sin 2\theta}{2}\right) |F(\sigma,\theta)|^2 \, d\theta \qquad (12)$$

$$S_{uw}(\sigma) = \int_0^{2\pi} K_u(\sigma) K_w(\sigma) \cos\theta \, |F(\sigma,\theta)|^2 \, d\theta \qquad (13)$$

$$S_{vw}(\sigma) = \int_0^{2\pi} K_u(\sigma) K_w(\sigma) \sin\theta \, |F(\sigma,\theta)|^2 \, d\theta \qquad (14)$$

where

$$K_u(\sigma) = \sigma \frac{\cosh k(h+z)}{\sinh (kh)} \qquad (15)$$

$$K_w(\sigma) = \sigma \frac{\sinh k(h+z)}{\sinh (kh)} \qquad (16)$$

$$K_p(\sigma) = \gamma \frac{\cosh k(h+z)}{\cosh (kh)}. \qquad (17)$$

For analyses of pressure/current meter data, equations involving u, v, and p subscripts, only, ((6)–(12)) are used to calculate the first five coefficients of a Fourier series representation of the directional spectrum:

$$a_0(\sigma) = \frac{1}{2\pi K_p^2(\sigma)} S_{pp}(\sigma) = \frac{1}{2\pi K_u^2(\sigma)} (S_{uu}(\sigma) + S_{vv}(\sigma)) \qquad (18)$$

$$a_1(\sigma) = \frac{1}{\pi K_p(\sigma) K_u(\sigma)} S_{pu}(\sigma) \qquad (19)$$

$$a_2(\sigma) = \frac{1}{\pi K_u^2(\sigma)} (S_{uu}(\sigma) - S_{vv}(\sigma)) \qquad (20)$$

$$b_1(\sigma) = \frac{1}{\pi K_p(\sigma) K_u(\sigma)} S_{pv}(\sigma) \qquad (21)$$

$$b_2(\sigma) = \frac{2}{\pi K_u^2(\sigma)} S_{uv}(\sigma). \qquad (22)$$

By employing a weighting function to eliminate negative side lobes in the directional distribution, the directional spectrum is calculated by

$$S(\sigma,\theta) = a_0 + \tfrac{2}{3}(a_1 \cos\theta + b_1 \sin\theta) + 1/6(a_2 \cos 2\theta + b_2 \sin 2\theta). \qquad (23)$$

The weighting function, also given by Longuet-Higgins *et al.* [8] is

$$W(\theta - \bar\theta) = \tfrac{8}{3} \cos^4 (\bar\theta - \theta)/2 \qquad (24)$$

with $\bar\theta$ the mean angle of the distribution. This function reduces directional resolution but does provide a more satisfying nonnegative distribution.

The acoustic triaxial current meter (UVW) analysis routine employs circular representations of wave directional spectral parameters using the auto- and cross-spectral relations given above which employ u, v, and w subscripts ((7)–(9), (12)–(14)). The directional energy spectrum is related to the one-dimensional spectrum by

$$S(\sigma,\theta) = S(\sigma) D(\sigma,\theta) \qquad (25)$$

where $D(\sigma,\theta)$ is a directional spreading function with

$$\int_0^{2\pi} D(\sigma,\theta)\, d\theta = 1. \qquad (26)$$

In this analysis, normalized Fourier coefficients are calculated according to Long [7]:

$$a_1(\sigma) = S_{uw}(\sigma)/[S_{ww}(\sigma)(S_{uu}(\sigma) + S_{vv}(\sigma))]^{1/2} \qquad (27)$$

$$a_2(\sigma) = (S_{uu}(\sigma) - S_{vv}(\sigma))/(S_{uu}(\sigma) + S_{vv}(\sigma)) \qquad (28)$$

$$b_1(\sigma) = S_{vw}(\sigma)/[S_{ww}(\sigma)(S_{uu}(\sigma) + S_{vv}(\sigma))]^{1/2} \qquad (29)$$

$$b_2(\sigma) = 2S_{uv}(\sigma)/(S_{uu}(\sigma) + S_{vv}(\sigma)) \tag{30}$$

and the directional distribution is given by

$$D(\sigma, \theta) = \frac{1}{2\pi}\,[1 + 2r_1 \cos(\theta - \theta_1) + 2r_2 \cos 2(\theta - \theta_2)] \tag{31}$$

where

$$r_1 = (a_1{}^2(\sigma) + b_1{}^2(\sigma))^{1/2} \tag{32}$$

$$r_2 = (a_2{}^2(\sigma) + b_2{}^2(\sigma))^{1/2} \tag{33}$$

$$\theta_1 = \arctan \frac{b_1(\sigma)}{a_1(\sigma)} \tag{34}$$

$$\theta_2 = \tfrac{1}{2} \arctan \frac{b_2(\sigma)}{a_2(\sigma)}. \tag{35}$$

Analysis of SXY data is based directly upon the Longuet-Higgins *et al.* [8] equations for the heave-pitch-roll buoy, but uses the differences in surface-corrected pressure records along the two perpendicular axes of the configuration to calculate $\partial\eta/\partial x$ and $\partial\eta/\partial y$ terms. Differentiating (1) with respect to x and y

$$\eta_x(x, y\ t) = \frac{\partial}{\partial x}\eta(x, y, t) = \int_{-\infty}^{\infty} \int_0^{2\pi} -i\,|k| \cdot \cos\theta F(\sigma, \theta) e^{i(k_x x + k_y y - \sigma t)}\, d\theta\, d\sigma \tag{36}$$

$$\eta_y(x, y, t) = \frac{\partial}{\partial_y}\eta(x, y, t) = \int_{-\infty}^{\infty} \int_0^{2\pi} -i\,|k| \cdot \sin\theta F(\sigma, \theta) e^{i(k_x x + k_y y - \sigma t)}\, d\theta\, d\sigma. \tag{37}$$

The co- and quad-spectra then appear as

$$S_{\eta\eta}(\sigma) = \int_0^{2\pi} |F(\sigma, \theta)|^2\, d\theta \tag{38}$$

$$S_{\eta_x\eta_x}(\sigma) = \int_0^{2\pi} -|k|^2 \cos^2\theta\, |F(\sigma, \theta)|^2\, d\theta \tag{39}$$

$$S_{\eta_y\eta_y}(\sigma) = \int_0^{2\pi} -|k|^2 \sin^2\theta\, |F(\sigma, \theta)|^2\, d\theta \tag{40}$$

$$S_{\eta_x\eta_y}(\sigma) = \int_0^{2\pi} -|k|^2 \cos\theta \sin\theta\, |F(\sigma, \theta)|^2\, d\theta \tag{41}$$

$$S_{\eta\eta_x} = \int_0^{2\pi} -i\,|k| \cos\theta\, |F(\sigma, \theta)|^2\, d\theta \tag{42}$$

$$S_{\eta\eta_y} = \int_0^{2\pi} -i\,|k| \sin\theta\, |F(\sigma, \theta)|^2\, d\theta \tag{43}$$

where

$$k_x = |k| \cos\theta, k_y = |k| \sin\theta. \tag{44}$$

The Fourier components of the directional distribution at a frequency band are then

$$a_0(\sigma) = \frac{1}{2\pi} S_{\eta\eta}(\sigma) \tag{45}$$

$$a_1(\sigma) = \frac{-1}{i\pi k} S_{\eta\eta_x}(\sigma) \tag{46}$$

$$a_2(\sigma) = \frac{1}{\pi k^2}(S_{\eta_x\eta_x}(\sigma) - S_{\eta_y\eta_y}(\sigma)) \tag{47}$$

$$b_1(\sigma) = \frac{-1}{i\pi k} S_{\eta\eta_y}(\sigma) \tag{48}$$

$$b_2(\sigma) = \frac{-2}{\pi k^2} S_{\eta_x\eta_y}(\sigma) \tag{49}$$

which are used in the unwindowed energy distribution over frequency and direction

$$S(\sigma, \theta) = a_0(\sigma) + a_1(\sigma) \cos\theta + b_1(\sigma) \sin\theta + a_2(\sigma) \cos 2\theta + b_2(\sigma) \sin 2\theta. \tag{50}$$

This approach is different than that normally used for processing SXY data as described by Higgins *et al.* [5]. There is also a step omitted to obtain sea-surface elevation from bottom pressure records.

Parameters to be compared in this paper are defined as follows.

1) Significant wave height $H_S \approx 4\sqrt{E_T}$, where

$$E_T = \int_0^{2\pi} \int_0^f S(\sigma, \theta)\, d\sigma\, d\theta. \tag{51}$$

2) Peak frequency f_p is the central frequency (in hertz) of the band containing the maximum energy, where frequency f is related to the angular frequency

$$\sigma = 2\pi f.$$

3) Peak wave direction θ_p, which is the mean direction of the frequency band containing maximum energy, where the mean direction is defined as

$$\bar{\theta} = \arctan \frac{b_1(\sigma)}{a_1(\sigma)}, \quad \text{for pressure/current gauges and SXY gauge} \tag{52}$$

$$= \tfrac{1}{2} \arctan \frac{b_2(\sigma)}{a_2(\sigma)}, \quad \text{for triaxial current meter.} \tag{53}$$

4) Peak directional spread θ_s, which is the estimated spread of energy about the mean wave direction at a fre-

quency, found by

$$\theta_s = (2 - [2(a_1{}^2(\sigma) + b_1{}^2(\sigma))^{1/2}/a_0(\sigma)])^{1/2}$$

for pressure/current gauges [3]

$$= (-\tfrac{1}{2} \ln r_2)^{1/2} \text{ for triaxial current meter [9].} \tag{54}$$

5)–6) Mean current speeds and directions are also compared for those instruments measuring horizontal currents, with a 1024 or 2048-s averaging interval.

B. Sources of Differences or Errors in Data

1) In Situ Measurements: Differences in directional wave characteristics measured by different instruments and processed with difference analysis software can be due to a variety of hardware and software dissimilarities, as well as dissimilarities in basic measurement philosophy (Tables III and IV). Clearly, the use of pressure sensors will lead to some different errors than those found with use of current meters; similarly, estimates of wave directions based on higher order Fourier coefficients will differ from those made using lower order coefficients (e.g., (34) and (35)). Because of the large number of sources, it is generally difficult to pinpoint specific reasons for differences in estimated wave parameters resulting from two measurement systems.

A comprehensive list of potential error sources and their estimated magnitudes (Tables III and IV) illustrates the need for extreme care in handling directional wave measurements, from system conception, to installation, and through analysis. Major sources of error include instrument specification, construction (machining) precision, installation, measurement of water depth and sensor position (including azimuth and inclination), electronic noise, and software considerations. Each is considered in turn below and quantified in Tables III and IV.

a) Specification errors: A directional wave system must include a number of critical specifications. Adequate spatial and temporal sampling must be assured. Resolution requirements (e.g., sample length in time for frequency resolution and statistical reliability requirements) need to be specified, as well as instrument precisions (especially true for instruments measuring surface gradients which rely on small differences between large numbers). Instruments must be fully calibrated throughout their performance range, preferably with the cumulative effects of the total system incorporated into the calibration (this is especially true for meters affecting the flow field they are trying to measure). Given sufficiently precise and well-understood instruments, the signal must be recorded in a manner preserving that precision (digital resolution or dynamic range requirement).

b) Construction deficiencies: An instrument must be constructed to minimize orientation uncertainties. For current meters, alignment particularly is critical (known travel path angles for acoustic current meters; accurate electrode placement for electromagnetic meters). Alignment between the oriented measuring device (current meter) and the orienting tool (external or internal compass and level indicators) must be well known and precision-machined. The orientation device and mount design should be simple yet stable for accurate, unobstructed flow measurements. Current meters commonly yield noncosine angular sensor response, which appeared to be present but of small effect in the gauges in this study. However, an investigator should be aware of the extent of this error [15].

c) Orientation errors: These result primarily from installation procedures, and can seriously degrade directional resolution and accuracy either through bias in the case of misalignment, or random fluctuations as in the case of an unstable tripod. Shallow water installations generally require divers to orient the sensor system. Errors in reading a compass underwater are on the order of two degrees, but depend on the type of compass used and readout capability. A compass deviation can be expected if the orientation measurement is made close to magnetic metals, a common occurrence for shallow water installations. These errors must be either avoided or corrected during analysis (by knowing the expected deviation due to the mooring device). For instruments measuring vertical velocity, field orientation is especially critical as contamination by horizontal velocity components can easily mask true vertical velocities. Vertical sensing better than 1° is difficult to achieve in the field; a 2° error in vertical alignment contributes a contamination of 3.5 percent of the horizontal velocity into the vertical velocity, resulting in a poor signal-to-noise ratio in near-bottom vertical velocity measurements. As shown by (27) and (29), orientation is particularly critical for an instrument sensing vertical velocity.

Quantization errors in internal compasses can also create significant errors. Eight-bit compasses result in a resolution of 1.4°. For unstable moorings, both compass resolution/accuracy and tilt resolution/accuracy (for vertical velocity measurements) can affect the precision of the directional measurements.

Mount motions are normally negligible during *in situ* gauge deployments. However, during ARSLOE, high waves occasionally broke near the deployment sites, rotating the CERC UVP gauge by 20°. The rotation was verified by diver observation and corrected for during data reduction. Vertical orientation of the gauge was not affected. The NHL UVW gauge's vertical axis was determined to be unstable during ARSLOE, and required correction during data analysis.

d) Depth errors: To correct for depth-dependent velocities and pressure, accurate knowledge of total water depth and instrument height is required. The biggest error here is usually uncertainty in sensor height. When sensing wave directionality by measuring vertical velocity, an independent measure of mean depth is required. Another error source is uncertainty in atmospheric pressure used for correcting bottom pressure measurements to sea-surface elevations. Error in this correction is generally small (order of a few centimeters).

e) Electronic factors: Behavior of electronics can affect sensor performance in a manner similar to biological fouling, low power conditions, clock inaccuracies and crosstalk between channels. Sampling format (instantaneous or integrated) can contribute aliasing errors; these were avoided here by using instruments with rapid sampling rates.

f) Software differences: Treatment of identical data

TABLE III
SOURCES OF DIFFERENCES AND POSSIBLE ERRORS AMONG *in situ* WAVE GAUGES

	NHL UVW	CERC UVP	WHOI UVP	CERC SXY
A) Specification Errors				
Accuracy of Sensor				
Calibration Errors				
Temporal Sampling Adequacy	Specification Errors Considered Negligible Compared to Other Categories; However, Reader Should Be Aware Of These Possible Errors In Specifying a Directional Gauge			
Spatial Sampling Adequacy				
Measurement/Recording Resolution				
B) Construction Deficiencies				
Sensor Alignment	±1° at best for all *in situ* instruments			
Mount Alignment (Machining)	±2° for most point gauges			Negligible
Sensor Interference	Negligible for all mount designs used in ARSLOE			
Cosine Response	Not Available	Maximum 5 percent Deviation in Velocity Measurement		Not Applicable
C) Orientation Errors				
Diver Compass Observation	±2° at best for all *in situ* instruments			
Compass Deviation by Magnetic Material	Negligible for the orientation techniques used			
Misalignment of Compass with Mount Axis	±1° at best for all *in situ* instruments			
Bubble Level	±1° at best for all *in situ* instruments			Not Applicable
Quantizing Error In Internal Compass	Internal Compasses Not Used		1.4°	Internal Compasses Not Used
Mount Motion	Mount motion is normally negligible if rigidly built and anchored. This can be verified during deployment by diver compass or internal compass.			
D) Depth Errors				
Measurement of Sensor Height	±10 cm resulting in a ±1 percent error wave height estimates (at 10-s wave period)			
Changes in Bottom Elevation	Changes of 50-cm result in wave height error estimates of <1 percent (for 10-s wave period)			
Sea Surface Elevation Measurements	Highly Dependent on Vertical Orientation	±1 percent in wave height estimates		
Inverse Barometric Effect	50-mm Hg change in pressure results in ±1 percent in surface elevation measurement			
E) Electronics				
Sensor Drift	Not Known	Amplitude Spectrum corrected for biofouling	Pre- and Post-Calibrations compare well	Not Known
Low Power Conditions	Did not occur during experiment period			
Inaccurate Internal Clock	Assumed Negligible	Not Applicable	Assumed Negligible	Not Applicable
Channel Cross-Talk	Did not occur during experiment period			
Sampling Scheme	Sampling Interval assumed small enough to allow satisfactory instantaneous or integrated schemes			
F) Software				
Computer Word Length	Error negligible for *in situ* analyses			
Quantizing Effects	Error negligible for *in situ* analyses			
Window Functions	Error negligible for *in situ* analyses			
Sampling Time Interval	Interval small enough to minimize aliasing out to cutoff frequency			
Time Sample Length	Longer sampling increases confidence (for given Δ, f) (see Section IV–C)			
Spectral Bandwidth	Uncertainty in peak Location of ±.0078 Hz			Uncertainty in peak of ±.0156 Hz
Spectral Averaging Scheme	No significant difference evident between ensemble averaging or band merging			
High/Low Frequency Cutoffs	0.40–0.012 Hz	0.36–0.010 Hz	0.25–0.008 Hz	0.40–0.012 Hz
	Range of 0.25 to 0.40 cutoff caused 5 percent average deviation in height			
Pressure/Velocity Transfer Functions	Monochromatic computations of storm wave conditions indicate underestimates of 12 percent in dynamic pressure and 11 percent in horizontal velocities using linear theory versus nonlinear stream function theory. Use of nonlinear response functions would increase the amplitude spectrum at lower frequencies, but would have no effect on the directional results.			

TABLE IV
IMAGING RADAR SYSTEM AND ANALYSIS ERROR

A) System Errors	
1. Motion of Waves During Sweep Time of Radar-Function of Wave Frequency	±1-2°
2. Selection of Mean Depth Over Wavelength (Affects Frequency Determination)—Function of Frequency and Nearshore Slope	±10 percent of wave period
B) Analysis Errors	
1. Angular Resolution of Radar	±1°
2. Protractor Resolution	±1.5°
3. Alignment Errors (Determining Reference Angle and Perpendicular to Wave Crests)	±5°
4. Errors in Measuring Wavelength Due to Resolution of Measurement Device, Clarity of Return, etc.	±5-10 percent of wavelength
5. Resolution of Dominant Wave Components from a Complex, Spectral Sea (Stationarity)	Unknown

sets with different computer hardware and software systems can produce disparate results. Because of aliasing and smearing problems, as well as wave-field stationarity, two important parameters are sample interval (Δt) and sample length (T). Computer word length and types (integer or real) can lead to roundoff or truncation errors which are important in spectral analysis where a large number of operations are performed. Windowing in both time and space can produce differences in analysis. Differences in averaging techniques are often small, but can lead to differences due to smearing and/or truncation/roundoff errors. When calculating variance, high- and low-frequency cutoffs are imposed in practice to limit the frequency band of interest to wind-driven surface gravity waves, and to reflect a high-frequency limit consistent with reasonable depth-corrected values of near-bottom pressure and velocity.

Since directional statistics can be defined in a number of different ways, definitions of relevant directional parameters were specified to each investigator to facilitate direct intercomparison of results. The analyses were in slight error through use of linear wave response functions.

2) Radar Measurements: Error analysis for imaging radar measurements is presented in some detail by Mattie and Harris [11]. Errors (Table IV) can be separated into two general categories: those associated with acquisition of the data versus those incurred during processing. Acquisition errors include angular resolution of the radar (about 1°), motion of waves during radar sweep time (error is a function of wave frequency), and clarity of radar trace. Processing errors arise from manual measurement of video images, and include resolution of measuring devices (protractors, rulers), estimation of mean depth over measurement site, and establishment of a reference angle for direction estimates. A further error source in directional statistics is representation of a random process by a single (or limited number of) photographic images.

IV. RESULTS AND DISCUSSION

Three types of comparisons are made between subsets of the directional wave gauges: time series of various wave parameters (III-A 1) to III-A 6)) outlined in Section III-A, detailed gauge-to-gauge statistical intercomparisons, and differences in spectral estimates resulting solely from analysis techniques.

A. Time Series Comparisons

Time series of six wave parameters were compared for different gauges: significant (zero moment) wave height, peak spectral wave frequency, peak wave direction, peak directional spread, mean current speed, and mean current direction. Figs. 4 and 5 present these parameters during two different time segments of ARSLOE, with lines drawn between points from the same gauge as an aid for following the temporal variation in measurements from each gauge.

Significant wave height data (Fig. 4) for all gauges (except the CERC radar which does not yield wave energy estimates) were intercompared along with a Baylor (resistance) gauge situated at the end of the FRF pier (Baylor data analyzed by CERC). Significant wave heights generally intercompare well, except those from the NHL UVW gauge. This lack of agreement may be due to problems in maintaining a stable (nonrotating) instrument mount and in ascertaining the depth at that gauge site because no direct sea-surface information was collected. However, because the trend in the NHL data matches that of other instruments (gauge-to-gauge comparison of the NHL UVW wave heights with those from other gauges for a large number of data points shows the NHL UVW heights to be low by a consistent proportion) indicating a more likely explanation may be that the gain was unacceptably low or a calibration factor was in error.

All gauges in this study, including the Baylor gauge, provide wave frequency data; time sequences of peak spectral frequency from *in situ* gauges and the measured wave frequency from the radar images are the basis for frequency intercomparisons (Fig. 4). Secondary peaks containing a large proportion of the energy are shown in the comparison as an additional point plotted concurrently with the peak frequency. Peak frequencies from the directional gauges and the Baylor appear to intercompare well. Three instances of secondary peaks are observed during the November time period by *in situ* gauges but not by the radar. This emphasizes the difficulty in visually assessing radar imagery of a complex sea sur-

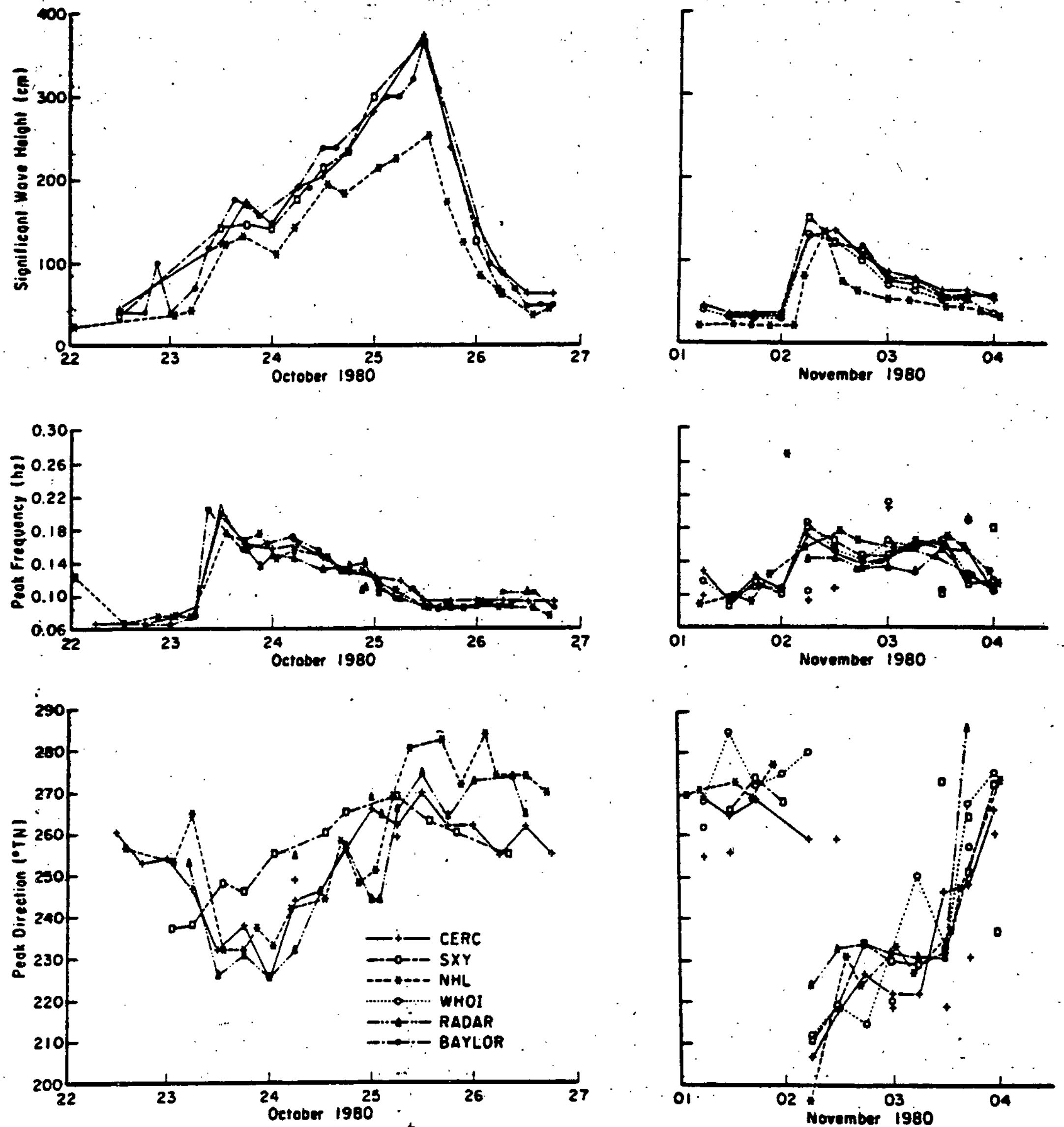

Fig. 4. Temporal comparison of significant wave height, peak wave frequency, and peak mean wave direction during two periods of ARSLOE.

for certain conditions; namely low wave height or two wave trains from approximately the same direction.

Peak wave direction versus time for the different instruments is presented as Fig. 4. Wave directions are spread over an average of about 20°, which is a larger deviation than expected from construction and orientation errors (about 5°), ~~but~~ reasonable in view of the number of instruments being compared. There are no distinctive trends in sensor deviation for the different systems. As observed for deep water waves by Kuik and Holthuijsen [6], the wind directions and wave directions are approximately equal in stationary onshore wind periods, while in slowly turning wind directions, the mean wave direction follows the onshore wind direction by a small time lag.

Comparison of peak wave directional spread versus time (Fig. 5) is based on different definitions of directional spread ((54) and (55)). This should not affect the intercomparison since the utility of the spread function is primarily in its representation of *trends* in spectral breadth. For example, the WHOI UVP analysis used a slightly different representation for the spread but shows a similar trend in spread during the November time period. Typical values of directional spread of 10°–15° during high-energy periods and 15°–20° during low-energy periods is lower than that found by van der Vlugt *et al.* [16] for deep water; this disparity is due in part to refraction effects as the waves propagate toward shore, narrowing the directional bandwidth.

Mean current direction and speed (Fig. 5) are defined by averages over the measurement period (T) of velocities sampled at equally spaced time intervals (Δt). Sample period and interval varied between gauges (Table II), but not enough to change the estimates of mean currents. Mean speed estimates are expected to be comparable since all sensors were located approximately 1 m from the bottom, placing them

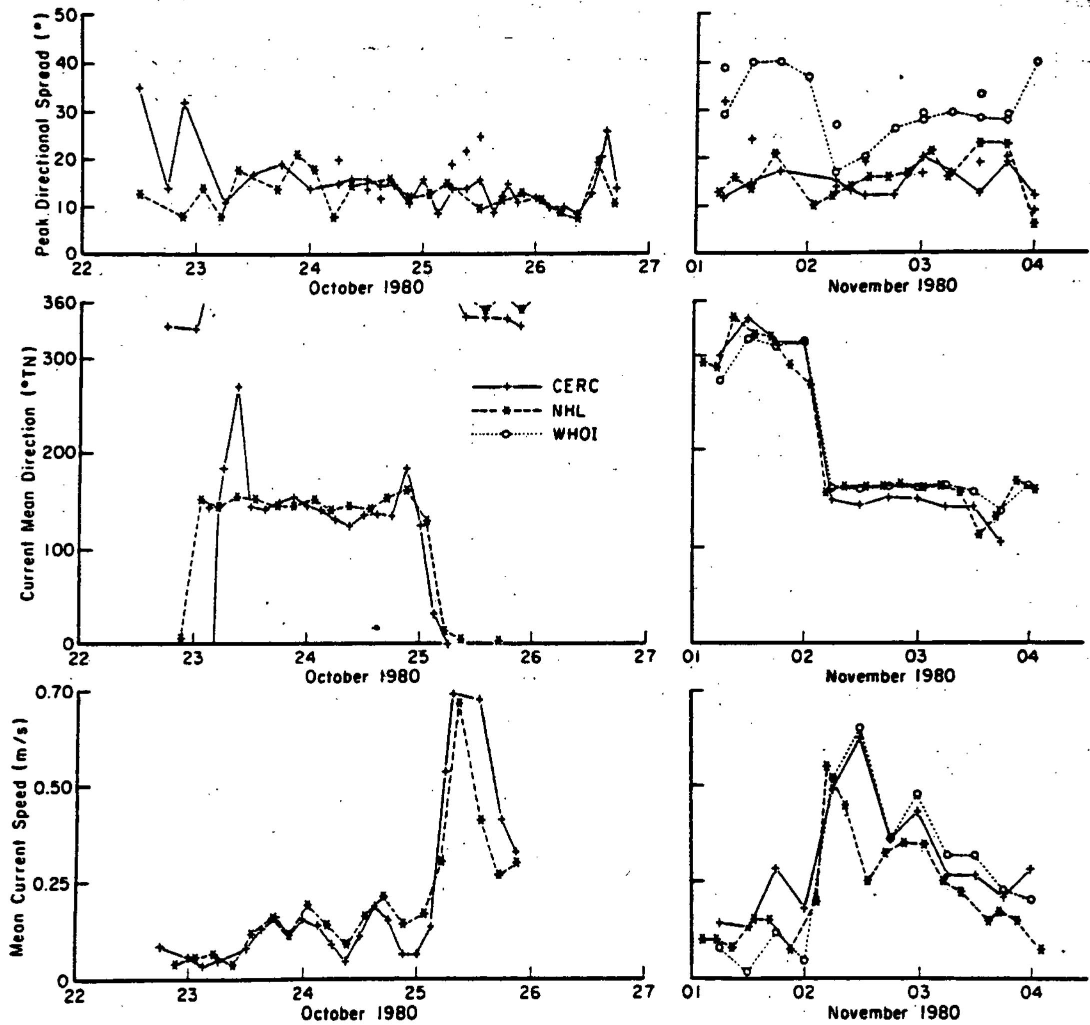

Fig. 5. Temporal comparison of peak mean directional spread, mean current speed, and mean current direction during two periods of ARSLOE.

in about the same part of the bottom boundary layer. Scatter in the current speed estimates reach 10 cm/s, but all meters show good agreement in trends. A significant deviation in flows occurred during the event on November 2, 1980, when the NHL UVW severely underestimated peak flows. A time-varying gain was applied to the CERC UVP current measurements to correct for biofouling-induced signal degradation during the warmer October records. In addition, a detailed calibration was available for only the WHOI UVP gauge at the time of this study.

B. Gauge-to-Gauge Statistical Comparisons

Gauge-to-gauge statistical comparisons were made between synoptic measurements (a lag of no more than 1 h 15 min between sample times) taken regularly throughout October and November, 1980. Some data points from the *in situ* gauges were not compared when the wave energy was extremely low, resulting in a low signal-to-noise ratio and poor estimates of wave direction. For multipeaked spectra (in frequency) only the peak under which the largest amount of energy resides was retained as the "peak" value. A radar data peak was chosen from a multipeaked case by retaining the peak closest in frequency to the major peak of the *in situ* gauges. The gauge-to-gauge statistical comparisons for the peak directional data are presented in Fig. 6 with the summary of comparison statistics shown in Table V.

The quantities intercompared between gauges were the mean direction associated with the peak frequency (as defined above), the peak frequency itself, and the significant wave height. Because each instrument was deployed for a different period of time, intercomparison linear regression statistics were generated based on a variable number of data points. Comparison between *in situ* gauges is generally good ($r^2 > 0.898$), while the correlation of the radar versus *in situ* gauges is somewhat less, but still high. As mentioned earlier, the processing of the radar images is dependent upon manual techniques at the present time and is subject to errors of ±3° to 5° inherent in manual measurements. The slopes and intercepts of the best fit lines of the radar versus several *in situ* gauges are nearly constant, indicating a constant bias to report the direction of the waves coming from the south (252° or greater) as more southerly than the other measurements. The data points of waves from northerly directions are evenly clustered about the 45° ideal best fit line (solid line in the plots). The average correlation coefficient of the radar versus *in situ* gauges of about 0.824 is close to that previously reported

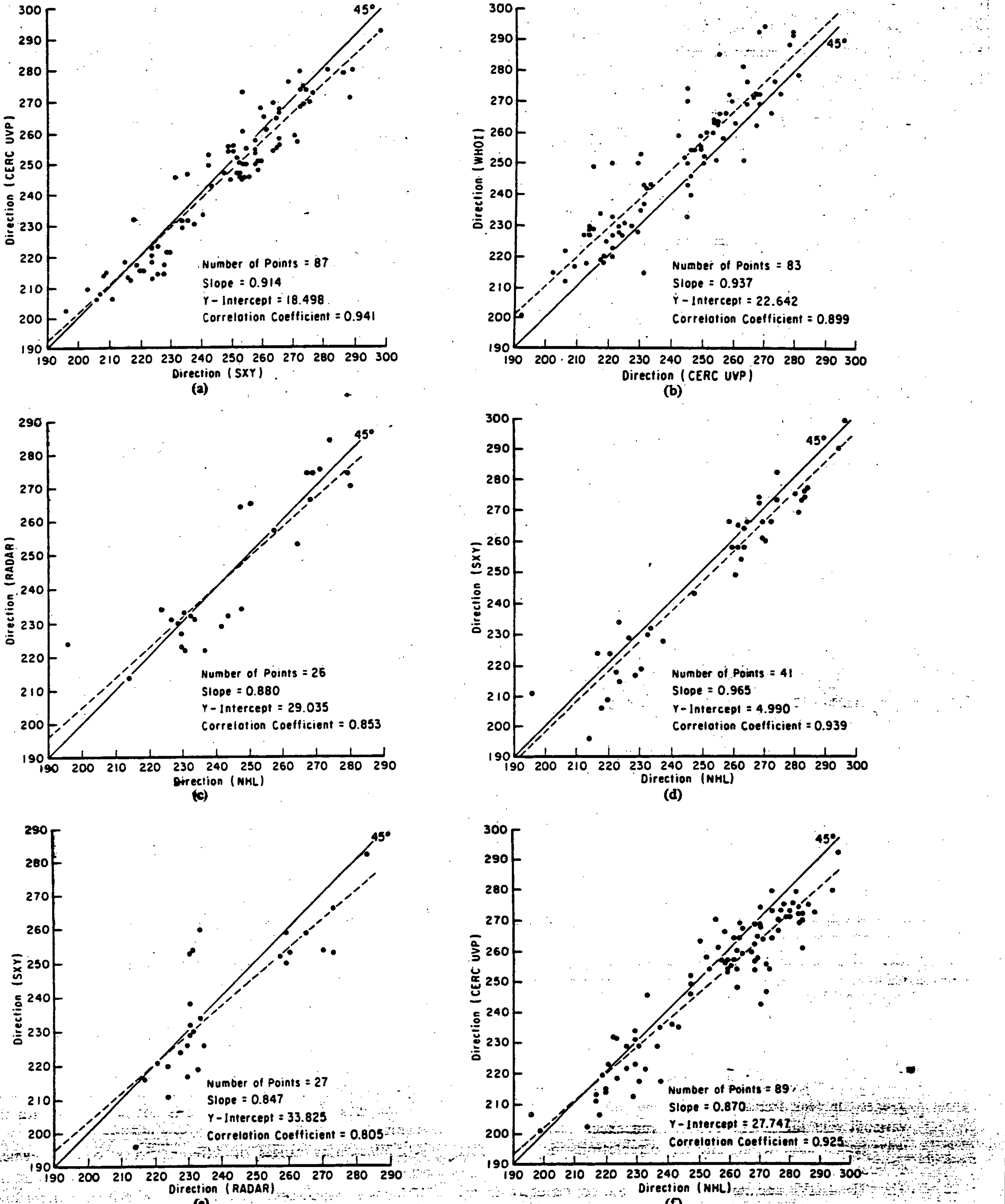

Fig. 6. Gauge versus gauge directional comparison for simultaneous data during ARSLOE.

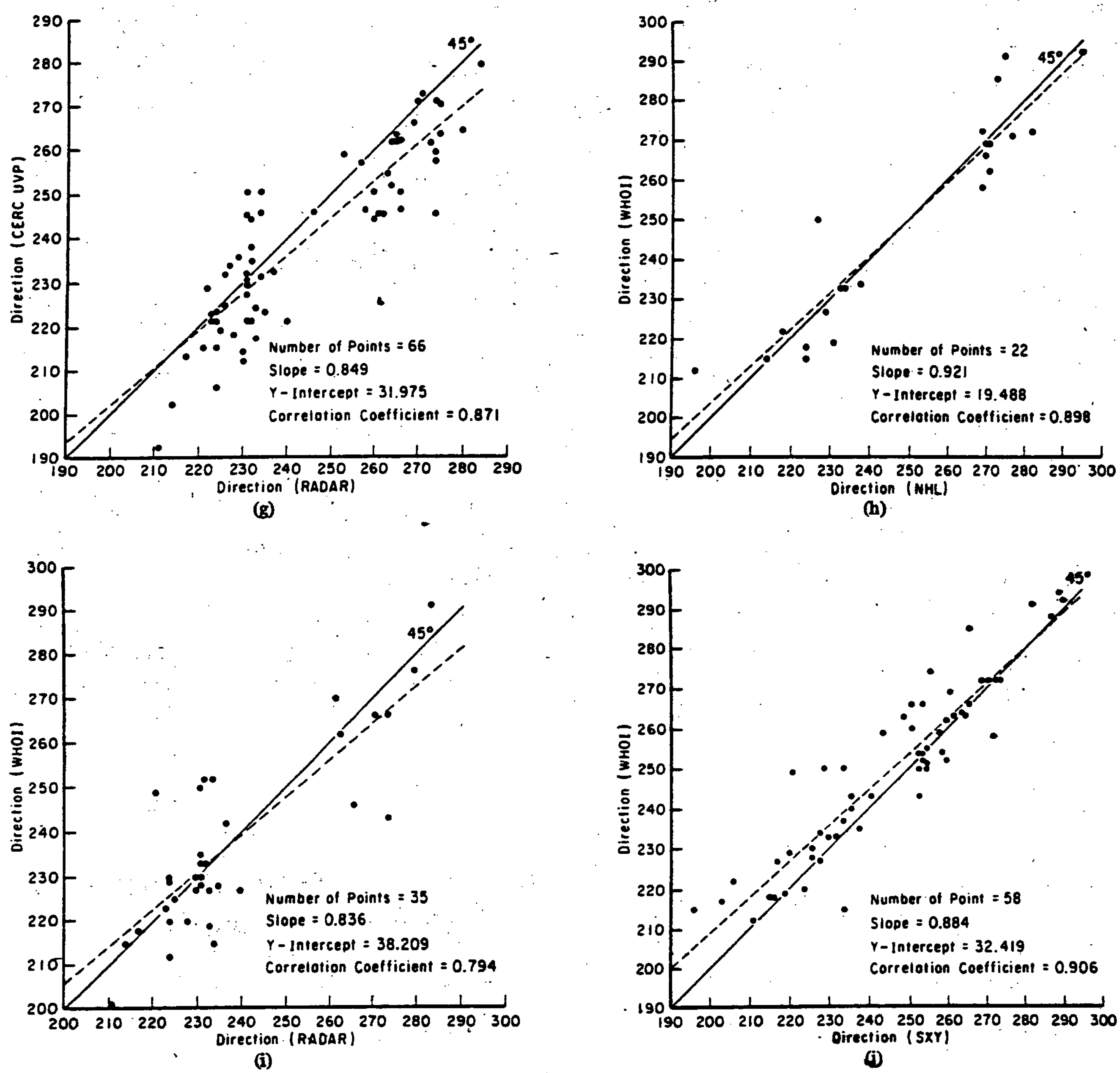

Fig. 6. *(continued)*

for the remote sensing radar and a side-looking airborne radar (SLAR) versus a pressure gauge array (Mattie *et al.* [12]).

The agreement between each *in situ* gauge with other *in situ* gauges appears to be consistent, with correlation coefficients averaging 0.928 for the SXY gauge, 0.922 for the CERC UVP, 0.921 for the NHL UVW, and 0.901 for the WHOI UVP. Note that the number of data points coincident between gauges is not constant with the statistics being more unreliable and variable for cases with low numbers of data points.

Tables VI and VII present correlation statistics between the gauges for peak frequency and significant wave height. Some variability in the frequency data and excellent agreement in wave height are evident. These two tables provide insight into differences due to gauge location, type, and analysis technique. The WHOI UVP and the SXY gages were colocated, with the UVP mounted above one leg of the SXY gauge; both use pressure data to provide the one-dimensional spectrum. High correlation and best fit statistics between these gauges are shown in the data. Disagreements in frequency and height are probably due to the differences in analysis programs (shown in Table III) or a low number of comparison points as in the case of the WHOI versus NHL comparisons. The wider bandwidth used in the SXY analysis alone can cause the type of disagreement in the frequency data.

No direct comparisons of the *in situ* instruments with the pier-mounted Baylor gauge were performed. However, data presented in Fig. 4 shows the peak frequencies measured by the Baylor gauge are slightly higher than the other gauges. The magnitude of the difference is not correlated with the magnitude of sea-surface variance.

In comparing gauges of different types, good agreement in most cases exists between CERC and WHOI UVP's and the SXY gauge, which use pressure records to provide surface one-dimensional spectral information. As seen earlier, however, directional correlations are not greater for comparisons of

TABLE V
COMPARISON OF PEAK DIRECTIONAL DATA (deg)

		(x) WHOI UVP	CERC UVP	CERC SXY	CERC Radar	NHL UVW
	WHOI UVP	–	$y = 0.937\ y + 22.6$ $r^2 = 0.899$ $N = 83$	$y = 0.884\ y + 32.4$ $r^2 = 0.906$ $N = 58$	$y = 0.836\ y + 38.2$ $r^2 = 0.794$ $N = 35$	$y = 0.921\ y + 19.5$ $r^2 = 0.898$ $N = 22$
	CERC UVP		–	$y = 0.914\ y + 18.5$ $r^2 = 0.941$ $N = 87$	$y = 0.849\ y + 32.$ $r^2 = 0.871$ $N = 66$	$y = 0.870\ y + 27.7$ $r^2 = 0.925$ $N = 89$
(y)	CERC SXY			–	$y = 0.847\ y + 33.8$ $r^2 = 0.805$ $N = 27$	$y = 0.965\ y + 5.$ $r^2 = 0.939$ $N = 41$
	CERC Radar				–	$y = 0.880\ y + 29.$ $r^2 = 0.853$ $N = 26$
	NHL UVW					–

TABLE VI
COMPARISON OF PEAK FREQUENCY DATA (Hz)

		(x) WHOI UVP	CERC UVP	CERC SXY	CERC Radar	NHL UVW
	WHOI UVP	–	$y = 0.979\ y + 0.003$ $r^2 = 0.947$ $N = 83$	$y = 0.936\ y + 0.007$ $r^2 = 0.955$ $N = 58$	$y = 1.03\ y + 0.009$ $r^2 = 0.806$ $N = 35$	$y = 0.857\ y + 0.024$ $r^2 = 0.845$ $N = 22$
	CERC UVP		–	$y = 0.932\ y + 0.008$ $r^2 = 0.983$ $N = 87$	$y = 1.03\ y + 0.003$ $r^2 = 0.914$ $N = 66$	$y = 0.816\ y + 0.022$ $r^2 = 0.876$ $N = 89$
(y)	CERC SXY			–	$y = 1.09\ y + 0.000$ $r^2 = 0.869$ $N = 27$	$y = 0.787\ y + 0.028$ $r^2 = 0.814$ $N = 41$
	CERC Radar				–	$y = 0.785\ y + 0.025$ $r^2 = 0.846$ $N = 26$
	NHL UVW					–

TABLE VII
COMPARISON OF SIGNIFICANT HEIGHT DATA (cm)

		(x) CERC UVP	CERC SXY	CERC Radar	NHL UVW
	WHOI UVP	$y = 1.00\ y - 10.0$ $r^2 = 0.980$ $N = 83$	$y = 0.973\ y - 3.2$ $r^2 = 0.977$ $N = 58$	N/A	$y = 1.20\ y + 14.8$ $r^2 = 0.770$ $N = 22$
	CERC UVP	–	$y = 0.967\ y + 8.7$ $r^2 = 0.980$ $N = 87$	N/A	$y = 1.24\ y + 9.4$ $r^2 = 0.954$ $N = 89$
(y)	CERC SXY		–	N/A	$y = 1.29\ y - 0.2$ $r^2 = 0.957$ $N = 41$
	CERC Radar			–	N/A

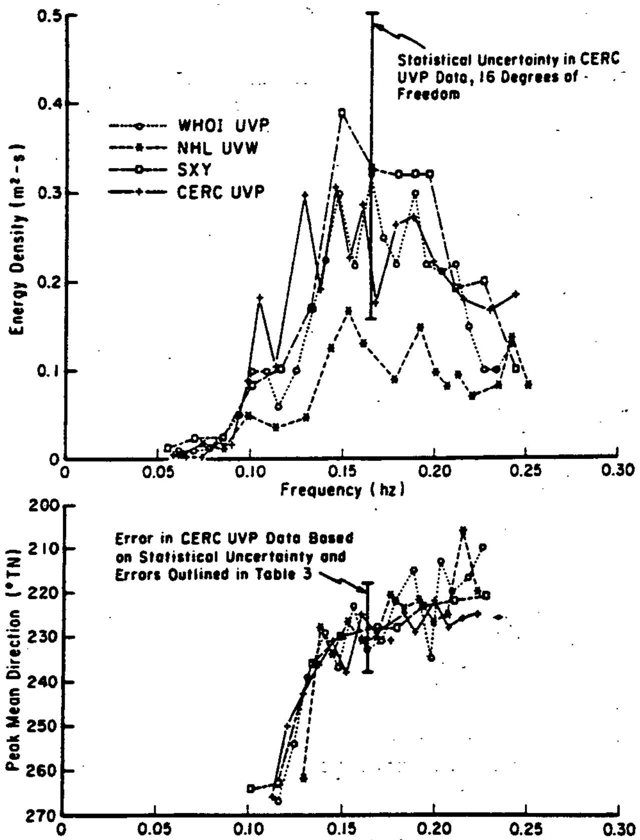

Fig. 7. Simultaneous energy and directional spectra from the nearshore *in situ* gauges collected on November 2, 1980 at 24:00 GMT. 90-percent confidence intervals for Figs. 7–10 have been shown for selected spectra. Ninety five percent confidence intervals for the remainder of the spectra are given by the following values: for estimates with 16 degrees of freedom, the expected value is within a factor of 0.55 and 2.32 of the sample value. For estimates with 32 degrees of freedom, the expected value is within a factor of 0.65 and 1.76 of the sample value.

similar gauges compared to those for dissimilar gauges, for gauges at similar locations versus those spaced further apart, or for gauges using similar analysis procedures versus those using more disparate techniques. The best-fit lines of the radar data versus the other gauges for frequency provide a good visual fit; however, because of the scatter in the data, the correlation coefficients are low. The NHL UVW (as mentioned earlier) changed orientation and the water depth was estimated (not measured); both factors probably contribute to the consistently lower wave height estimates. Disregarding the case of the NHL versus WHOI comparisons where very few simultaneous records were collected, all correlation coefficients in wave height are above 0.95 and above 0.80 for peak frequency.

C. Observations of Differences in Spectral Data

As mentioned earlier, all *in situ* instruments provide both energy and directional spectra for each record of wave data collected. Because the gauges are located in a small area, comparison of simultaneous spectra provides insight into differences in results due to analysis programs, instrument location and gauge type.

Samples of analyzed data collected simultaneously by a subset of the gauges are presented in Fig. 7. The figure contains an energy density spectrum along with a plot of the mean wave direction versus frequency. The plot is a sample of particular analyzed synoptic data records and cannot be interpreted as a comprehensive comparison between gauges. The spectral shapes are slightly different, with the primary peaks at slightly different frequencies, possibly due to differences in record lengths, sampling frequencies, averaging technique, and, in the case of the SXY gauge, bandwidth. Fig. 8 further illustrates the variability in spectral estimates due to differences in analysis programs. The WHOI analysis program uses an ensemble averaging technique and averages over 16 subsamples. When the same data record is analyzed by the CERC program (which merges 16 frequency bands), an energy distribution is produced with a shift in the peak location of one band. The variation in the two sets of data analyzed by the CERC routine might suggest that the peak does in reality shift slightly and a small shift of energy being transferred from higher to lower frequencies between gauge locations, but more likely is insignificant because this variation is within the confidence interval of the spectra.

Fig. 9 further investigates the effect of record length on the spectral results, where the WHOI analysis routine was run on complete 2048-s records and then on the first 1024-s of the same record. The total variance is slightly higher in the 1024-s case which also is more irregular with several more pronounced minor peaks.

Fig. 10 presents three spectra from the CERC UVP in both energy and direction with radar data points plotted on the same axes. The first case is a single peaked case as indicated by the UVP; however, the radar shows it as doubled peaked, with two wave trains arriving at very similar frequencies but almost 25° apart in direction. This illustrates the tendency for *in situ* analysis techniques to provide an average direction based on energy weighting when two or more wave trains are occurring that are too close in frequency to be adequately resolved. Here it appears that two wave trains of equal energy caused a peaked energy spectrum, while the direction measured by the CERC UVP was approximately the mean of the two radar measurements.

The second case shows a double peaked spectrum where the peaks are well separated and closely represented by both the radar and UVP. A single peaked case is also included with results again agreeing between the two techniques.

V. CONCLUSIONS

Five directional wave gauges (dissimilar in either design, manufacturer, or concept) were deployed and maintained for a portion of the two-month ARSLOE experiment during 1980. All were located within 200 m from one another, in a wave field varying spatially due to wave shoaling (refraction and shallow water propagation) and structural interference (from the adjacent FRF research pier). Fetch and duration varied insignificantly between the wave gauges.

Differences in wave estimates from the different gauges were the combined result of a variety of factors, from design specification differences to software idiosyncracies. In general, the different instruments intercompared well, with trends

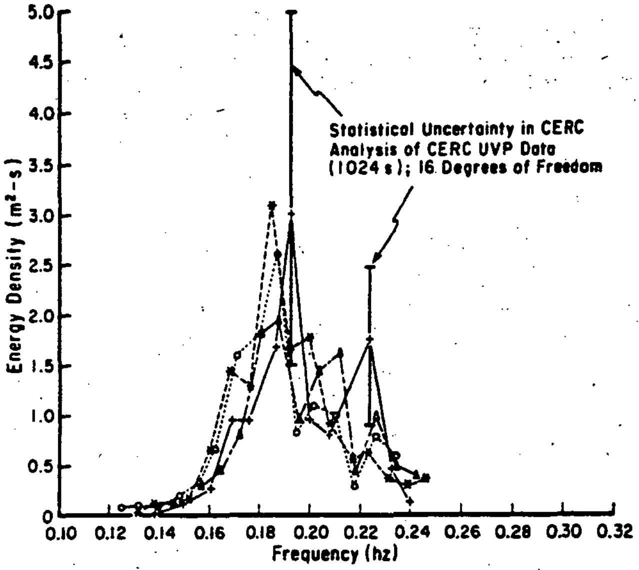

Key	Data	Analysis Program	Total Energy (m²)	Peak Direction (°TN)	Peak Frequency (hz)	Gage Depth (m)	Mean Current Speed (m/s)	Mean Current Direction (°TN)	Record Length (s)	Sampling Frequency (hz)
—+—	CERC UVP	CERC	0.137	207	0.191	5.71	0.196	150	1024	4
—*—	WHOI UVP	CERC	0.131	211	0.184	7.33	0.209	163	2048	1
···o···	WHOI UVP	WHOI	0.111	212	0.183	7.33	0.209	163	2048	1
--+--	WHOI UVP	WHOI	0.101	210	0.183	7.29	0.199	163	1024	1

Fig. 8. Comparison of wave data processed by the CERC and WHOI analysis programs, varying the record length and sampling frequency.

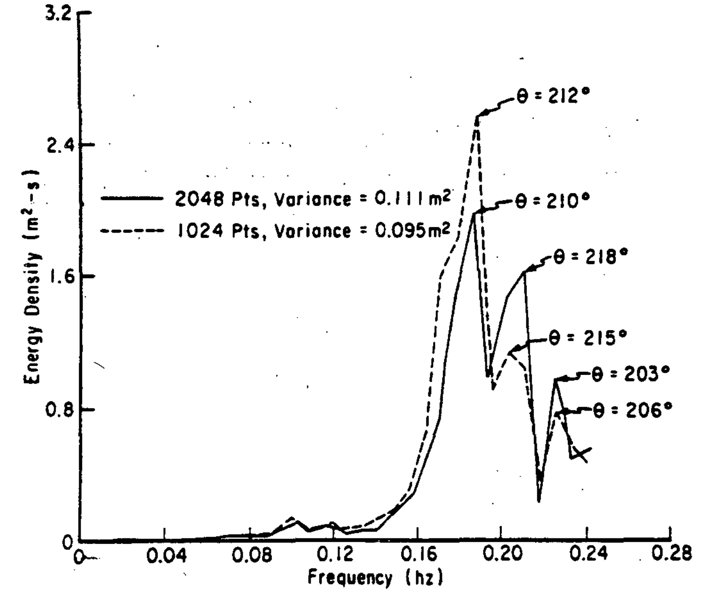

Fig. 9. Comparison of the effect of record length on the energy and directional spectrum.

in directional, frequency, and energy content well correlated between gauges through time. Specific differences did exist.

1) The NHL UVW gauge differed in energy content from other gauges by almost a constant proportion. This was probably a result of an error in gain for the vertical data channel. The experimental results emphasize the need for an independent measure of mean sea surface elevation when using a UVW combination, and the difficulty of obtaining a stable vertical reference.

2) The CERC radar did not always successfully identify multidirectional wave components at different frequencies. Conversely, the radar can often identify two direction peaks at a similar (nearly identical) frequency, whereas the other wave gauges generally averaged the two directions together. This lack of resolution is a theoretical problem, however; by redefining peak selection criteria, the UVP and UVW gauges are able to identify separate peaks at a given frequency. This lack of resolution is a limitation to the Fourier model fit for directional wave estimation.

3) The Baylor gauge, situated on the FRF pier, yielded slightly higher peak frequencies than any other gauges on October 24–25, for unknown reasons. Possible explanations for this observation could be software differences, or the "red shift" associated with shoaling wave spectra (the Baylor Gauge is located in deeper water than the other gauges). There was no direct relationship between the magnitude of the frequency shift and the sea-surface variance (Fig. 4).

4) Wave directional spreads show similar trends through time, in spite of the different representations used to define angular variability.

5) Spectral estimates generated by ensemble averaging and band merging show no characteristic differences, for samples where the number of bands merged equals the number of ensembles averaged (equal equivalent degrees of freedom). Small shifts (±1 band) in peak frequency did occur as a result of the averaging differences.

6) Spectral estimates for a fixed frequency bandwidth (0.0078125 cps) and with different sample lengths (hence degrees of freedom) showed some differences for the periods

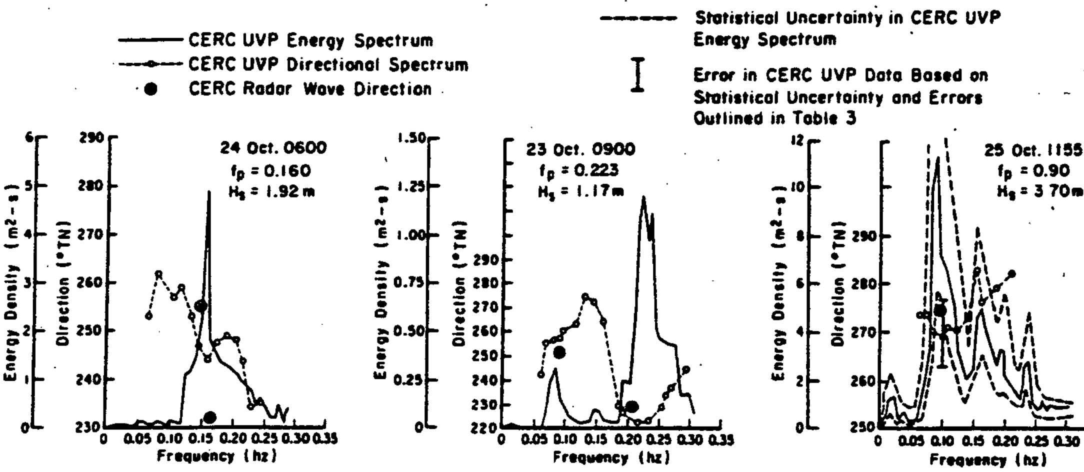

Fig. 10. Investigation of radar analysis results versus *in situ* data.

compared in this analysis. Variances are slightly larger for the 1024-s case (17.1 min) than for the 2048-s case (34.2 min). Peak frequencies may also shift slightly between the two cases. Finally, the 1024-s spectra show multiple peaks not present from longer samples (as would be expected given the differences in degrees of freedom). This observation suggests that for many applications a shorter (17.1-min) record may be sufficient to characterize the sample spectrum for wave conditions similar to those at the FRF. For other circumstances, however, the shorter record may not be sufficient.

VI. SUMMARY

For types of *in situ* gauges and a radar with their associated analysis schemes provide comparable wave directional data. The *in situ* gauges utilizing a pressure sensor provided a better estimate of the surface energy spectrum than the gauge using vertical velocity data. An advantage of the *in situ* measurements is the ability to resolve multiple wave trains of different frequency coming from close to the same direction, which is difficult with the radar. The radar, however, can resolve multiple wave trains of similar frequency coming from different directions, while the *in situ* gauges provide an energy weighted average direction at that frequency. Present radar analysis techniques also have inherent uncertainties which should be considered when using such a system. Better processing techniques can increase the capability of *in situ* devices to detect multiple trains.

Errors and uncertainties which might occur in data from the *in situ* instruments have been outlined; most can be avoided if proper care is taken in designing, building, and deploying the gauges. Analysis software will also influence the results. Better directional estimates are achievable through use of more sophisticated data analysis procedures (data adaptive methods, for instance).

ACKNOWLEDGMENT

This work benefited from the cooperation of the many participants in the Atlantic Remote Sensing Land Ocean Experiment which was hosted jointly by the U.S. Army Corps of Engineers and the National Oceanic and Atmospheric Administration. Personnel at the U.S. Army CERC Field Research Facility actively supported the field operations required for this study.

The Corps of Engineer research contained in this paper was conducted as part of the Coastal Flooding and Storm Protection Research Program, Coastal Engineering Functional Area, of the Civil Works Research and Development Program of the U.S. Army Corps of Engineers. Permission to publish this paper was granted by the Chief of Engineers.

REFERENCES

[1] D. G. Aubrey, "Field evaluation of sea data directional wave gage (Model 635-9)," Woods Hole Oceanographic Inst., Tech. Rep. WHOI-81-28, May 1981.

[2] L. E. Borgman, "Directional wave spectra from wave sensors," in *Ocean Wave Climate*, M. D. Earle and A. Malahof, Eds. New York: Plenum, 1979, pp. 269–300.

[3] D. E. Cartwright, "The use of directional spectra in studying the output of a wave recorder on a moving ship," in *Ocean Wave Spectra*. Englewood Cliffs, NJ: Prentice-Hall, 1963, pp. 203–218.

[4] W. G. Grosskopf, "Computer algorithm to calculate a wave direction spectrum and related parameters from a biaxial current meter and a pressure gage," Coastal Eng. Res. Center Category "A" Computer Program and Documentation, Coastal Engineering Res. Center, Ft. Belvoir, VA, Nov., 1981.

[5] A. L. Higgins, R. J. Seymour, and S. S. Pawka, "A compact representation of ocean wave directionality," *Appl. Ocean Res.*, vol. 3, no. 3, pp. 105–111, 1981.

[6] A. J. Kuik and L. H. Holthuijsen, "Buoy observation of directional wave parameters," in *Proc. Conf. Directional Wave Spectra Applications*, R. L. Wiegel, Ed., Amer. Soc. Civil Eng., Sept. 14–16, 1981, pp. 61–70.

[7] R. B. Long, "The statistical evaluation of directional spectrum estimates derived from pitch/roll buoy data," *J. Physical Oceanography*, vol. 10, pp. 944–952, 1980.

[8] M. S. Longuet-Higgins, D. E. Cartwright, and N. D. Smith, "Observations of the directional spectrum of sea waves using the motions of a floating buoy," in *Ocean Wave Spectra*. Englewood Cliffs, NJ: Prentice Hall, 1963, pp. 111–132.

[9] K. V. Mardia, *Statistics of Directional Data*. London and New York: Academic, 1972.

[10] M. Mathiesen and T. Faanes, "Directional wave spectra from the Frigg Field in the North Sea," Norwegian Hydrodynamic Lab. Rep. 2-82092, 1982.

[11] M. G. Mattie and D. L. Harris, "A system for using radar to record wave direction," U.S. Army Corps of Engineers, Coastal Engineering Res. Center Tech. Rep 79-1, Sept. 1979.

[12] M. G. Mattie, S. V. Hsiao and D. D. Evans, "Wave direction measured by four different systems," *IEEE J. Oceanic Eng.*, vol. OE-6, pp. 87–93, July 1981.

[13] D. P. McCann, D. M. Cotter, A. A. Punchak, and D. E. Lichy, "Atlantic remote sensing land ocean experiment—ARSLOE," in *Proc. Wave Dynamics and Radar Probing of the Ocean Surface*, IVRCM, Miami, FL, May 1981.
[14] R. J. Seymour and A. L. Higgins, "Continuous estimation of longshore sand transport," in *Proc. Coastal Zone '78*, vol. III, pp. 2308–2318, 1978.
[15] J. D. Smith, "Measurement of turbulence in ocean boundary layers," in *Proc. Conference on Current Measurment*, Tech. Rep. DEL-SG-3-78, W. Woodward, C. N. K. Mooers, and K. Jensen, Eds., College of Marine Studies, Univ. of Delaware, Newark, DE, 1971.
[16] A. J. M. Van der Vlugt, A. J. Kuik and L. H. Holthuijsen, "The WAVEC directional buoy under development," in *Proc. Conf. Directional Wave Spectra Applications*, R. L. Wiegel, Ed., Amer. Soc. Civil Eng., Sept. 14–16, 1981, pp. 50–60.
[17] L. Baer and C. L. Vincent, "Atlantic remote sensing land/ocean experiment (ARSLOE): Overview," *IEEE J. Oceanic Eng.*, this issue, pp. 201–205.

★

William G. Grosskopf was born in Niagara Falls, NY, on December 22, 1955. He received the B.C.E. and M.C.E. degrees from the University of Delaware, Newark, in 1977 and 1979, respectively. His work at the graduate level concentrated on coastal and ocean engineering.

He has been with ARCTEC, Inc., Columbia, MD, since mid-1982, where his concentration has been in wave hindcasting, storm surge modeling, and the siting of coastal structures based on wave and sedimentation effects. The work has involved physical, analytical and numerical modeling of ocean and coastal systems. He has also designed, constructed and deployed oceanographic measurement systems, particularly in the area of directional wave and current monitoring in shallow coastal areas. During 1980–1982 Mr. Grosskopf worked as a hydraulic engineer at the US Army Corps of Engineers Coastal Engineering Research Center (CERC), Ft. Belvoir, VA. There he participated in shallow water wave attenuation and tidal modeling efforts, as well as in the development of a shallow water directional wave measurement and analysis system for CERC.

★

David G. Aubrey was born in Fort Sill, OK, Claremont, CA, on August 21, 1950. He received B.S. degrees in civil engineering and geological sciences from the University of Southern California, Los Angeles, in 1973, and completed the Ph.D. degree in oceanography at Scripps Institution of Oceanography, Claremont, CA, in 1978.

He is presently an Associate Scientist at Woods Hole Oceanographic Institution, Woods Hole, MA, concentrating in the areas of nearshore processes, shelf sediment transport, waves and currents, beach erosion, and tidal inlets. His interests in the measurement of ocean and coastal processes have led him to study and evaluate various oceanographic measurement systems and analysis techniques.

★

Michael G. Mattie, photograph and biography not available at time of publication.

★

Martin Mathiesen, photograph and biography not available at time of publication.